Interactions between model organic compounds and metal oxides

Noor Zaouri, Leonardo Gutierrez, Marc F. Benedetti, Jean-Philippe Croué

Interactions between model organic compounds and metal oxides

Submitted to

Colloids and Surfaces A: Physicochemical and Engineering Aspects

February 2021

Noor Zaouri[1], Leonardo Gutierrez[2,3], Marc F. Benedetti[4], Jean-Philippe Croue[3*]

[1] Water Desalination and Reuse Center, King Abdullah University of Science and Technology, Saudi Arabia

[2] Facultad del Mar y Medio Ambiente, Universidad del Pacifico, Ecuador

[3] Université de Poitiers, Institut de Chimie des Milieux et des Materiaux IC2MP UMR 7285 CNRS, France

[4] Université de Paris, Institut de Physique du Globe de Paris, UMR 7154, CNRS, Paris, France

* Corresponding Author:

Email address: jean.philippe.croue@univ-poitiers.fr

Telephone: +33 (0)5 49 36 62 83

32 pages, 6 Figures, 3 tables, and a Supporting Information section are included in the current manuscript.

Abstract

Because of their mechanical, thermal, and chemical resistance, ceramic materials are suitable for challenging water treatments, where different metal oxides (MeO) have been tested as active layers. However, organic fouling is a major drawback impacting its performance. Organics adsorb onto the membrane surface and into their pores during long-term operation, resulting in irreversible fouling. This investigation focussed on the interfacial interactions between model organic acids and MeO to obtain a fundamental understanding of the adsorption phenomena. Batch adsorption experiments of a series of small molecular weight, oxygenated, aromatic organic acids were performed with Al_2O_3, TiO_2, and ZrO_2 particles, at pH 4.2 and 7.6. The adsorption of simple acids was described by the Langmuir model and exhibited a strong dependence on the relative abundance of carboxyl groups, aliphaticity/aromaticity, alkyl chain length, and presence of hydroxyl groups. The adsorption of model compounds was higher at low pH and decreased with increasing pH. The difference in Al_2O_3, TiO_2, and ZrO_2 surface characteristics, as evidenced by TEM, XRD, and BET, led to differences in the adsorption density. The results obtained with these well-defined organic structures will assist in better understanding the interfacial interactions between complex natural organic matter molecules and MeO of different characteristics.

Keywords: adsorption**,** metal oxide, Langmuir isotherm, pH point of zero charge, small organic acids.

1. Introduction

Ceramic membranes are currently used in a broad range of applications, e.g., drinking water treatment, food industry, urban and industrial wastewater treatment [1, 2]. Because of their mechanical, thermal, and chemical resistance, ceramic materials are suitable for challenging water treatments (e.g., hazardous waste, oil/water separation, and industrial effluents); thus, providing the advantage of extended membrane lifespan even after severe fouling and cleaning conditions [3]. However, organic fouling is still a major drawback impacting its performance [4, 5]. Despite periodic physical cleaning or chemically-enhanced backwashing (CEB), some organics adsorb onto the membrane surface and into the membrane pores during long-term operation, resulting in permeability loss and irreversible fouling [5-7]. Consequently, controlling irreversible fouling associated with organics (e.g., Natural/Effluent Organic Matter-NOM/EfOM) adsorption is essential to improve the performance of membrane processes.

Organic matter (OM) is ubiquitous in natural and industrial process waters and is generally present as a heterogeneous mixture of small molecules (a few hundred Daltons) and moderate to high molecular weight (MW, above 20 KDa) structures [8]. Parameters commonly used to characterize NOM include elemental analysis, acidity, charge, functional groups, aromatic character with fluorophores distribution, and specific ultraviolet absorbance (SUVA) [9]. NOM is enriched with hydroxyl and carboxyl functional groups that confer high solubility in water. For instance, humic substances (HS) consist of molecules that form aggregates via intermolecular forces and vary between mono- to hexacarboxylic acids, short-chain aliphatic mono- to polycarboxylic acids, long-chain fatty acids, and phenolic carboxylic acids [9-11].

Metal oxides (MeO, e.g., iron oxide, alumina oxide, and manganese oxide) have been investigated under different approaches to prevent or minimize ceramic membrane (organic)

fouling, as pre-adsorbents (particles in suspension) or active layers [12]. Previous studies on the interaction between NOM and MeO have focused on the influence of pH, electrolytes, type of MeO, and type and concentration of organic compounds in the adsorption process. These works have investigated the basic adsorption mechanisms and extent of adsorption of organic matter onto metal oxides, pH dependency, the relative affinity of various organic compounds for a specific surface, and binding mechanisms. Briefly, based on NMR and FTIR analysis, carboxylic and phenolic groups incorporated in NOM structure are important in the adsorption on MeO surfaces [13-16]. The heterogeneous and unique composition of humic and fulvic acid controls the adsorption behavior and binding mechanisms on goethite surfaces, as proved by the Ligand and Charge Distribution (LCD) model [17]. Also, different MeO surface properties (i.e., surface charge and density) showed a significant influence on the adsorption profile of NOM molecules and small aromatic carboxylic acids [18, 19]. Remarkably, MeO surfaces of high pH_{PZC} (point of zero charge) have shown high adsorption capacities (e.g., ZrO_2) [18, 19]. Although most of the investigations have focussed on the adsorption of complex NOM molecules on MeO, their interaction mechanisms as a function of their physicochemical characteristics are still not clear. Specifically, NOM structures incorporate many different reactive sites in addition to uncharacterized components; thus, influencing and adding a level of complexity to the elucidation of these interfacial interactions with different MeO surfaces [20].

As a consequence, several comprehensive studies have correlated the adsorption of NOM on MeO with the adsorption of well-defined small organics already identified in the structure of NOM. For instance, Evanko and Dzombak (1998) studied the adsorption of benzoic acids incorporating different numbers of carboxylic acids and the influence of the acidity variation in NOM adsorption on goethite surface [20]. Dobson and McQuillan (1999, 2000) studied the

impact of different chemical structures (i.e., aliphatic and aromatic organic acids) in the adsorption mechanism on alumina oxide, titanium oxide, zirconium oxide, and tantalum pentoxide [18, 21]. Hwang and Lenhart (2008) studied the effect of the molecular structure and the orientation of the carboxyl group in the adsorption of small C4-dicarboxylic acid molecules on hematite particles [22].

The current study focussed on the adsorption kinetics and adsorption isotherms between eleven organic acids and three different MeO surfaces. The adsorption profile was analyzed based on the characteristic of both organic acids and MeO surfaces. The organic acids (i.e., covering a wide range of characters and structures) were selected as representative low MW aliphatic and aromatic acid moieties incorporated in the complex NOM matrix and were analyzed by High-Pressure Liquid Chromatography (HPLC). Three MeO surfaces (i.e., as microparticles) were selected based on their relevance as microfiltration ceramic membrane active layers and coatings, i.e., alumina oxide (Al_2O_3), zirconium oxide (ZrO_2), and titanium oxide (TiO_2). Each MeO surface was rigorously characterized using sensitive techniques. The impact of pH on: a) the surface characteristics of MeO (pH_{PZC}) and organics (pKa) and b) their interfacial interactions were investigated. The results obtained with these well-defined organic structures will assist in better understanding the interfacial interactions between NOM and MeO of different characteristics.

2. Material and Methods

2.1. Metal Oxide (MeO) Particles and Model Organic Compounds

Three types of MeO were investigated: alumina oxide (Al_2O_3), zirconium oxide (ZrO_2), and titanium oxide (TiO_2) (ϕ: 125-250 µm, Kerafol Company, Germany). The MeO particles were washed with a 0.1 M NaOH solution and then thoroughly rinsed with Milli-Q water. All MeO

particles were calcinated at 900˚C for 8 hours under atmospheric conditions. Based on their treatment process, these particles mainly represent microfiltration ceramic membranes. The phase of each MeO after calcination was identified by XRD (section 2.3.3).

Eleven polar aliphatic and aromatic compounds of different properties (e.g., chemical structure, acidity constants-pK_a, functional groups) were selected as model organic compounds (Figure 1). The selection of these model compounds was conducted to study a) the difference in interactions between MeO and aliphatic or aromatic structures (i.e., as well as the influence of the length of the aliphatic chain), and b) the contribution of carboxyl and hydroxyl groups on these interactions.

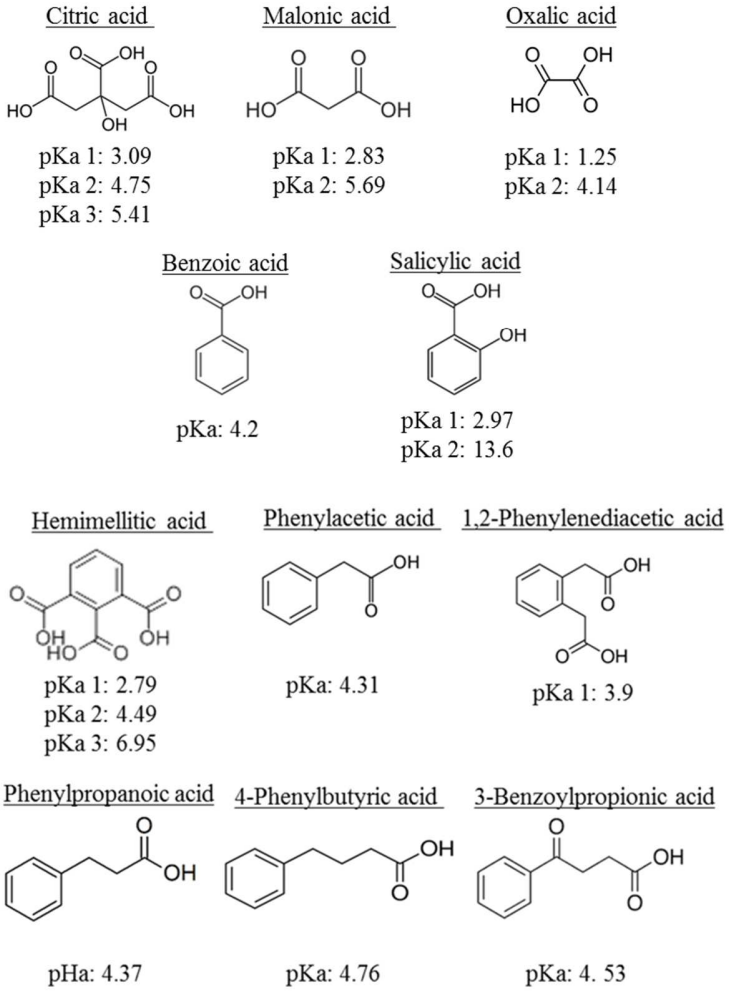

Figure 1: Chemical structure and pKa of selected model compounds

2.2. Experimental methods

Batch experiments (i.e., adsorption kinetics and adsorption isotherms) were conducted at acid and nearly neutral pH. MeO particles were equilibrated in Milli-Q water for 24 h before experiments.

2.2.1. Adsorption kinetics

Adsorption kinetics experiments were conducted in 500 ml glass bottles containing 3 g/L MeO particles (i.e., Al_2O_3, TiO_2, or ZrO_2). The organic compound solutions were prepared in 0.01 M $NaClO_4$ at pH 4.2 and pH 7.6. The pH was adjusted with 0.1 M HCl and with 0.1 M of NaOH. The initial concentration of aliphatic acids, aromatics, and aromatic acids with aliphatic chains was 0.2 mM, 0.05 mM, and 0.044 mM, respectively. The solutions were mixed using an overhead shaker for five days at room temperature (21°C). On the first day, samples were collected after 5 min, 10 min, 40 min, 1 h, 8 h, and 12 h of contact time. Samples were then collected every 8 and 12 hours for five days. The adsorption rate constant (K_s) was calculated as per equation 1.

$$K_s = \frac{C_t - C_0}{t\, C_0\, m\, A} \qquad (1)$$

Where C_0 is the initial concentration of the organic compound (µmol/L), C_t is the organic compound concentration (µmol/L) at time t (hour), m is the mass of MeO (g), and A is the specific surface area of the MeO (m^2/g).

2.2.2. Adsorption isotherm

MeO particles were added at a dose ranging from 0 to 5 g/L, to 15 mL of the model organic compound solution prepared in 0.01 M $NaClO_4$ at pH 4.2 and pH 7.6. Batch adsorption

147 experiments were conducted at different initial concentrations of the model organic compounds
148 (i.e., from 0.05 to 0.2 mM) in plastic centrifuge tubes. The suspensions were mixed for 72 hours
149 to reach adsorption equilibrium (i.e., verified for all compounds) using an overhead shaker at
150 room temperature (21 ℃). The residual concentrations of organic compounds were determined by
151 High-Performance Liquid Chromatography (HPLC). The amount of adsorbed organic acids per
152 surface area of MeO was calculated by the difference between the initial concentration and the
153 concentration after equilibrium (72 hours), following equation 2:

154 $$q = \frac{(C_0 - C_e)V}{Am} \qquad (2)$$

155 Where q is the amount of adsorbed organic per surface area (µmol/m^2), C_0 is the initial
156 concentration of organics (µmol/L), C_e is the concentration of organics at equilibrium (µmol/L),
157 V is the solution volume (L), A is the specific surface area of the MeO sample (m^2/g), and m is
158 the mass of MeO particles (g). The adsorption density for each organic compound was calculated
159 by fitting the adsorption isotherm data with the Langmuir model (eq. 3 and 4). After rigorous
160 analysis, Langmuir model was selected among other models to describe the adsorption of these
161 small acids.

162 $$\text{Langmuir isotherm: } q = \frac{q_{max}\, K\, C_e}{1+(K\, C_e)} \qquad (3)$$

163 $$\text{Linear form: } \frac{1}{q} = \frac{1}{q_{max}\, K\, C_e} + \frac{1}{q_{max}} \qquad (4)$$

164 Where q is the mass of solute adsorbed per mass of MeO (µmol/m^2), q_{max} is the maximum
165 adsorption (µmol/m^2), K is the adsorption affinity constant [13, 23], and C_e is the equilibrium
166 concentration (µmol/L).

167 **2.3. Analytical methods for model organic compounds and MeO characterization**

168 **2.3.1. Potentiometric proton titration**

The titration of the MeO particles was performed in a jacketed glass beaker under a constant temperature by using a circulating water bath (25˚C). Two electrodes connected to a computer (i.e., a Metrohm 6.0133.100 glass and a single 6.0733.100 reference electrode) were used to record the pH values. The pH electrodes were calibrated by performing a blank titration in the background electrolyte. The titration of the suspensions was conducted by adding small volumes of titrant while recording the pH of the solution. Titration experiments were performed on 20 ml of Milli-Q water containing 2 g of MeO particles. The solutions for each MeO sample were purged with pure N_2 gas to avoid the interference of CO_2. The ionic strength was adjusted with a concentrated 5 M $NaNO_3$ solution to reach a final concentration of 0.01, 0.1, and 1 M. The pH was controlled during titration by the addition of 0.1 M HCl and 0.1 M NaOH previously prepared with degassed Milli-Q water. After each addition, a drift value of pH was calculated (mV/min). The maximum time for acquiring each data point was set to 30 min. A similar approach was followed for the blank test.

2.3.2. Chemisorption/Temperature-Programmed Desorption (TPD)

The basic and acidic sites of the three MeO samples (Al_2O_3, TiO_2, or ZrO_2 particles) were measured by Chemisorption tests. The Carbon Dioxide Temperature-Programmed Desorption (CO_2-TPD) process was conducted to measure the basic sites using a Micromeritics AutoChem 2950 instrument equipped with a TPD. Briefly, the MeO sample was placed into a U-shape quartz tube and pre-treated at 150°C under helium flow (40 ml/min) for 60 mins. When the temperature was decreased to 50°C, CO_2 sorption was performed by flowing 10% CO_2 in helium (50 ml/min) for 30 mins. Then, the sample was purged under helium flow (40 ml/min) for 45 mins. Finally, the desorption experiment was performed by purging helium gas (50 ml/min) and ramping the temperature from 50 to 1000°C at a rate of 10°C/min. For measuring the acidic sites,

192 the NH_3-TPD test was performed using the same experimental procedure while replacing the
193 10% CO_2 in helium with 10% NH_3 in helium.

194 **2.3.3. Transmission Electron Microscopy, X-Ray Diffraction, and BET analysis**

195 The MeO samples were analyzed by a High-Resolution Bright-Field Transmission Electron
196 Microscope (HR-BF-TEM), performed on a Titan CT (FEI, The Netherlands) operated at 300 kV
197 and equipped with a Charge-Coupled Device (CCD) camera (Gatan Inc.). Multiple locations of
198 the specimens were investigated. An XRD Bruker D8 Advance was used to confirm the nature
199 and purity of the MeO sample, as well as its crystallinity form. Each sample was scanned from
200 10° to 90° (2θ) in steps of 0.02°. BET (Brunauer, Emmett, and Teller) analysis was conducted to
201 measure their specific surface area.

202 **2.3.4. Analyses of model organic compounds by High-Pressure Liquid Chromatography**

203 All solutions were filtered using a 0.45 µm glass fiber syringe filter to remove MeO particles. A
204 Waters HPLC Model 1525 equipped with a bridging HPLC pump and UV detector was used to
205 measure the concentration of the model compounds. A calibration curve was individually
206 prepared for each organic acid with concentrations ranging from 0.5 to 200 µM. The operation
207 condition for each organic acid detection is listed in Table S1.

208 **3. Results and discussion**

209 **3.1. MeO properties**

210 ZrO_2 particles showed the highest surface area (10.1 ± 0.14 m^2/g) compared to TiO_2 (5.6 ± 0.1
211 m^2/g) and Al_2O_3 (3.8 ± 0.07 m^2/g). The pH_{PZC} of ZrO_2 and Al_2O_3 was determined as 7.5 and 8.8
212 (Table S2 and Figure S1), respectively. Although these values are in good agreement with others
213 found in the literature [24], the pH_{PZC} of TiO_2 was higher than previously reported pH_{PZC}, i.e., 8.9
214 vs. 5 to 6 [24, 25], possibly due to the intensive cleaning and thermal treatment applied. Previous

studies have shown that TiO_2 phase transformation (rutile-anatase) depends on the synthesis conditions, i.e., temperature, hence shifting the pH_{PZC} [26-28]. According to XRD and EDX results, all MeO samples (i.e., Al_2O_3, TiO_2, or ZrO_2) were pure (Figure S2-S3). The crystallinity of the particles was identified by XRD and was also supported by high-resolution TEM images (Figure S3). All MeO samples were characterized by Miller indices, referring to the family of lattice planes (e.g., anatase) [29]. ZrO_2 showed a monoclinic phase structure with (110) and (101) planes [30]. TiO_2 was identified as a tetragonal phase structure with (101) planes, while corundum showed a hexagonal phase, and an (11-20) plane was identified for Al_2O_3.

The density of the active sites detected on each MeO is listed in Table 1. The strength of the sites was determined by the desorption temperature of CO_2 and NH_3. The higher the desorption temperature, the higher the strength of the site.

Table 1. Surface concentration of basic and acidic sites on MeO particles

Temp. (°C)	**Acidic sites (µmol/m²)**	**Temp. (°C)**	**Basic sites (µmol/m²)**
Al_2O_3			
363.0	8.85	23.60	2.03
576.0	7.22	19.25	8.14
842.6	3.67	**-**	-
TiO_2			
237.7	17.46	**-**	-
375.3	14.61	**-**	-
581.8	6.31	**-**	-
810.2	4.23	**-**	-
ZrO_2			
291.5	2.45	17.43	0.24
466.2	5.31	37.77	0.33
757.4	2.45	**-**	-

Al_2O_3 and ZrO_2 showed basic and acidic sites of different strengths. Three acidic sites and two basic sites of different strengths were detected in both MeO based on the desorption temperature.

230 On the other hand, TiO_2 only showed four acidic sites on its surface (Table 1). The absence of
231 basic sites on the TiO_2 surface would be due to the treatment of the particles with NaOH and
232 900°C calcination that could result in different TiO_2 material (e.g., rutile) [26]. As indicated in
233 many studies, Jung et al. (2001) reported that calcination temperatures exert a major influence on
234 the density of surface sites [31]. The different densities and strength of the sites on MeO surfaces
235 have been previously correlated to the difference in the crystallographic structure, calcination
236 temperature, and material type [30-32].

237
238
239 3.2. **Adsorption kinetics of model organic acid compounds**

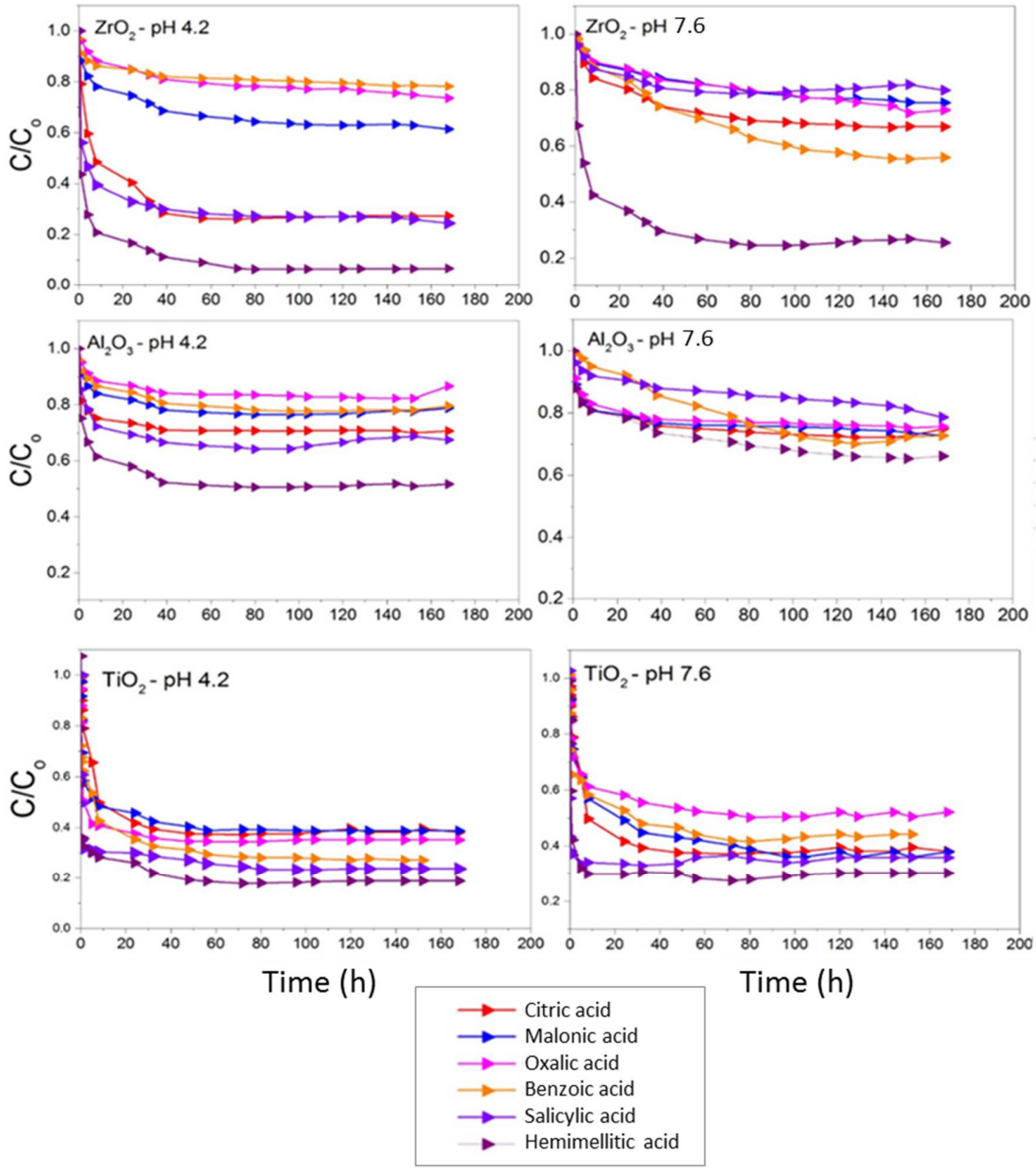

240

241 **Figure 2.** Adsorption kinetics of carboxylic acids and phenylacetic acids on TiO_2, Al_2O_3, and
242 ZrO_2 at pH 4.2 and 7.6.

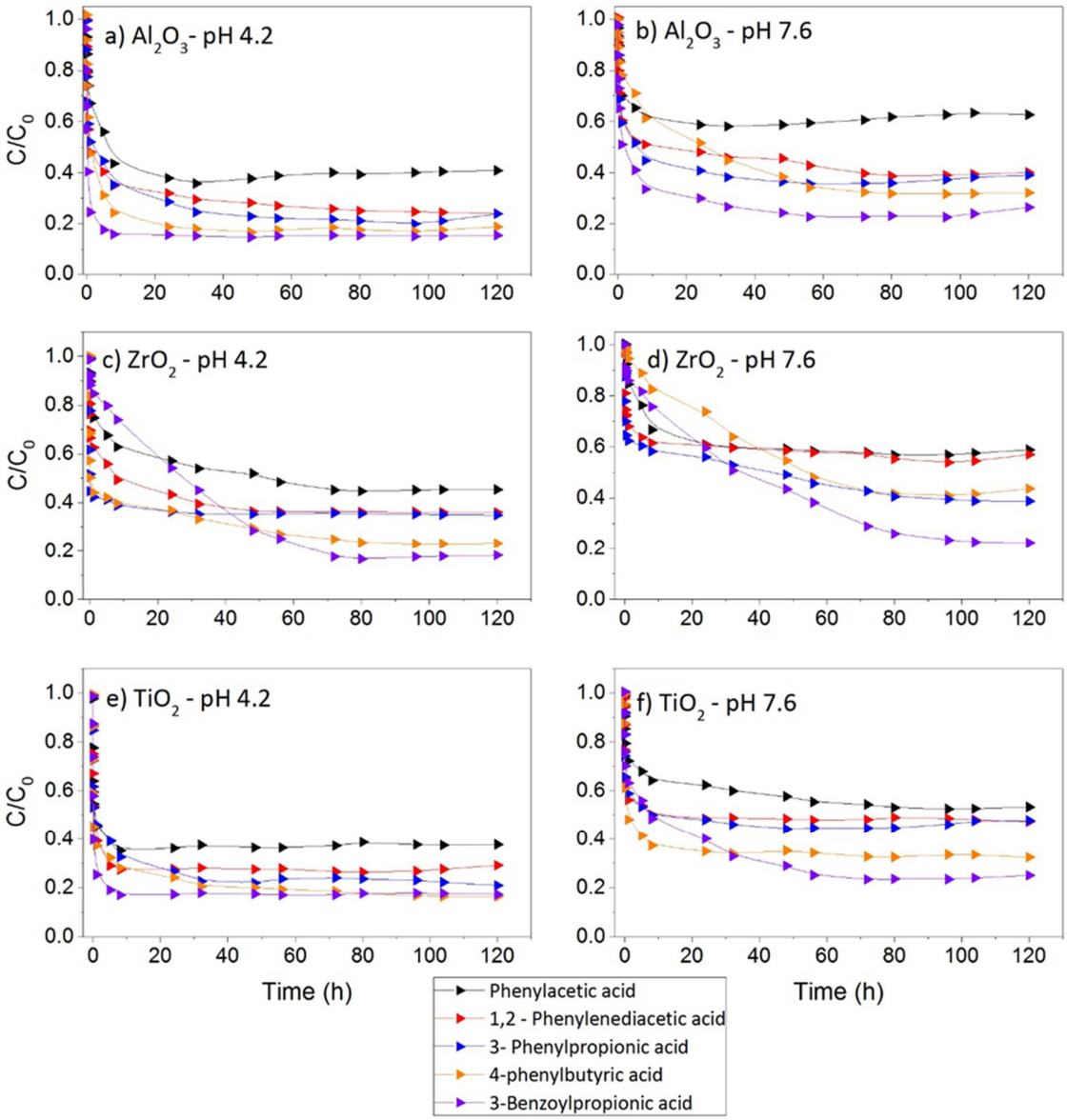

Figure 3. Adsorption kinetics of phenyl carboxylic acids on TiO_2, Al_2O_3, and ZrO_2 at pH 4.2 and 7.6.

According to the adsorption kinetics in Figures 2 and 3, a few days of contact time were necessary to reach adsorption equilibrium for all MeO samples with organics at acidic and neutral pH. Hence a contact time of 72 hours was selected to conduct the adsorption isotherm experiments. Furthermore, the kinetics were controlled by the pH for all studied compounds with all MeO samples. Increasing the pH from 4.2 to 7.6 resulted in a significant decrease in K_s (i.e.,

initial adsorption rate constant calculated in the first hour of reaction) with all MeO samples (Table S3), except for oxalic and malonic acids with ZrO_2 and Al_2O_3, where an increase in pH led to an increase in K_s (Table S3). At pH 4.2, the general trend showed that K_s-TiO_2 and K_s-Al_2O_3 > K_s ZrO_2, except for salicylic acid, where its highest K_s value was recorded with ZrO_2. For 1, 2-phenylenediacetic acid, and 3-benzoylpropionic acid, K_s values were significantly higher with Al_2O_3 than with the other two MeO samples. For phenylpropionic acid, its K_s value was significantly higher with TiO_2 than with the other two MeO samples. At pH 7.6, the general trend indicated that ZrO_2 always showed the lowest K_s values, except with 4-phenylbutyric acid. Also, K_s-TiO_2 > K_s-Al_2O_3 for all compounds, except for oxalic acid, malonic acid, 3-phenylpropionic acid, and 1, 2-phenylenediacetic acid. A similar investigation correlated the influence of pH on the decrease of the surface charge of goethite, hematite, and α-alumina samples, impacting the adsorption mechanism, and hence, the adsorption kinetics [20, 22, 33, 34].

The pH of the solution can significantly affect the adsorption kinetics by changing the ionization state of the MeO surface and the organic acid molecules [35]. Due to their high pH_{PZC}, all MeO samples were positively charged in the experiments conducted at pH 4.2. For experiments conducted at pH 7.6, the surface of ZrO_2 would approach the pH_{PZC}, while Al_2O_3 and TiO_2 remained positively charged. Similarly, the functional groups in the structure of the organic acids have different pK_a; thus, causing protonation/deprotonation as a function of solution pH. Therefore, the diversity of the surface properties of MeO and the chemical structure and composition of organic acids induce a wide range of interactions that influenced the adsorption kinetics, as previously observed between small acids and TiO_2, ZrO_2, Ta_2O_5, hematite, Al_2O_3, and iron oxides [18, 21, 22, 35, 36].

When organic compounds show similar acidic character, aromatic acids exerted a stronger interaction in comparison to aliphatic acids. The results indicated that the characteristics of the functional groups attached to the aromatic ring have a significant influence on the adsorption kinetics [20] (Figures 1 and 2). Specifically, the adsorption mechanism is controlled by the chemical structure [18, 20]. Dobson and McQuillan (1999, 2000) reported different adsorption mechanisms of aliphatic and aromatic acids on TiO_2, Al_2O_3, ZrO_2, and Ta_2O_5. Briefly, the adsorption of acetic acid on the ZrO_2 occurred via the formation of a surface chelate structure. Both benzoic and acetic acid have similar acidic character (i.e., monocarboxylic acids) and formed bidentate coordinated benzoate species on ZrO_2 [18, 21]. However, the adsorption of benzoic acid to ZrO_2 would follow interfacial solvent water displacement, as suggested by Dobson and McQuillan (1999). Besides, the increase in the acidity in the benzoic ring by an additional carboxyl group exerts a stronger influence on the kinetics than an OH group, i.e., salicylic and hemimellitic acid [20]. The results indicated that hemimellitic acid showed the fastest initial adsorption rate at both pH conditions and for all MeO. However, these differences were more important at acidic pH than at basic pH. Still, salicylic acid showed a high K_s value at pH 4.2. Possibly, the presence of a non-charged OH group (i.e., OH or COOH groups) positioned on the aromatic structure would increase the adsorption rate at acidic pH [20, 37]. Remarkable trends were observed for oxalic and malonic acids (i.e., small C2 and C3 di-acids) compared to citric acid (C6 tri-acid). Oxalic and malonic acids showed fast kinetics with ZrO_2 and Al_2O_3 at pH 7.6. At this pH, both acids are fully dissociated (i.e., as the other acids); however, their smaller size might favor their diffusion to available positive sites.

Aromatic structures with a single carboxyl group (i.e., salicylic and benzoic acids) showed a different behavior than aromatics with attached fatty acid chain structures at both pHs and with

297 all MeO. Specifically, the conformation of the molecule is an important factor governing the
298 adsorption kinetics. Increasing the length of the fatty acid chain attached to aromatic moiety
299 leads to faster adsorption through enhancing the interaction of the carboxyl group at low pH (i.e.,
300 which decreases with increasing pH) [20].

301 ### 3.3. Adsorption isotherms of model organic acid compounds

302 **Table 2:** Langmuir adsorption isotherm parameters of phenyl carboxylic acids calculated from
303 Equation 3.

*q_{max}: µmol/m^2	pH 4.2			pH 7.6				
	q_{max}*	K	R^2	q_{max}*	K	R^2	$q_{max\ 4.2}/q_{max\ 7.6}$	$K_{4.2}/K_{7.6}$
	ZrO_2							
Phenylacetic acid	1.04	2.81	0.91	0.99	2.28	0.91	1.05	1.23
1,2-Phenylenediacetic acid	1.52	3.14	0.98	0.93	0.59	0.94	1.63	5.32
Phenylpropanoic acid	1.63	0.21	0.91	1.55	2.61	0.96	1.06	0.08
4-Phenylbutyric acid	3.59	0.09	0.91	1.14	2.63	0.89	3.15	0.03
3-Benzoylpropanoic acid	1.44	0.37	0.98	0.94	0.65	0.88	1.53	0.57
	Al_2O_3							
Phenylacetic acid	3.16	2.94	0.99	2.66	1.32	0.92	1.19	2.22
1,2-Phenylenediacetic acid	4.02	1.36	0.94	3.24	0.26	0.93	1.24	5.16
Phenylpropanoic acid	3.99	0.67	0.85	3.92	0.84	0.8	1.02	0.81
4-Phenylbutyric acid	4.72	2.42	0.93	3.06	0.41	0.94	1.54	5.84
3-Benzoylpropanoic Acid	7.24	0.12	0.94	4.45	0.81	0.93	1.63	0.15
	TiO_2							
Phenylacetic acid	1.16	1.45	0.82	0.52	0.71	0.94	2.23	2.03
1,2-Phenylenediacetic acid	2.26	0.68	0.95	2.02	1.06	0.92	1.12	0.65
Phenylpropanoic acid	1.71	0.87	0.96	1.23	0.49	0.9	1.38	1.80
4-Phenylbutyric acid	3.87	0.30	0.92	2.02	14.18	0.83	1.91	0.02
3-Benzoylpropanoic Acid	3.04	0.63	0.9	1.95	0.15	0.94	1.56	4.29

304

305

306 **Table 3:** Langmuir adsorption isotherm parameters of carboxylic acids and phenylcarboxylic
307 acids calculated from Equation 3.

	ZrO_2							
*q_{max}: µmol/m²	pH 4.2			pH 7.6				
	q_{max}*	k	R^2	q_{max}*	k	R^2	$q_{max4.2}/q_{max\ 7.6}$	$K_{4.2}/K_{7.6}$
Citric acid	6.08	0.29	0.87	1.31	0.66	0.91	4.64	0.44
Malonic acid	1.31	0.88	0.97	0.76	0.37	0.89	1.72	2.4
Oxalic acid	1.58	0.8	0.85	2.18	0.13	0.99	0.72	6
Benzoic acid	0.27	3.31	0.94	0.39	15.45	0.91	0.69	0.21
Salicylic acid	1.44	0.25	0.88	0.88	1.11	0.92	1.64	0.23
Hemimellitic acid	1.99	0.33	0.98	1.48	0.25	0.91	1.34	1.34
	Al_2O_3							
Citric acid	6.64	0.25	0.87	3.49	1.59	0.87	1.9	0.16
Malonic acid	1.08	11.56	0.85	1.19	9.9	0.9	0.91	1.17
Oxalic acid	0.71	2.16	0.85	0.96	44.44	0.87	0.74	0.049
Benzoic acid	0.29	3.08	0.85	0.19	13.47	0.83	1.53	0.23
Salicylic acid	0.67	14.37	0.87	0.62	17.14	0.86	1.08	0.84
Hemimellitic acid	1.25	11.09	0.94	1.13	5.04	0.89	1.11	2.2
	TiO_2							
Citric acid	5.45	0.2	0.91	2.55	0.85	0.93	2.14	0.24
Malonic acid	2.15	1.19	0.87	1.01	0.47	0.93	2.13	2.55
Oxalic acid	1.95	0.28	0.97	0.75	0.04	0.97	2.6	6.45
Benzoic acid	0.95	0.36	0.83	0.45	1.35	0.85	2.11	0.26
Salicylic acid	1.45	1.31	0.96	1.02	1.02	0.88	1.42	1.28
Hemimellitic acid	2.51	0.19	0.98	1.45	1.93	0.89	1.73	0.1

308

309 The fitted data for all compounds and MeO samples at both pH 4.2 and 7.6 showed a high
310 correlation coefficient (R^2), indicating the suitability of the Langmuir model for the current
311 system (Figures S4 and S5). The adsorption density (i.e., reported as q_{max}) clearly decreased with
312 increasing pH (Tables 2 and 3). This observation has been reported in similar studies where the
313 adsorption density of trimellitic and hemimellitic acid with Al_2O_3 and benzoic acid interactions

with goethite decreased with increasing solution pH [20, 23]. Balistrieri and Murray (1987) observed that the adsorption of oxalic, phthalic, salicylic, and lactic acids on goethite increased with decreasing pH [38]. Also, Conroy et al. (2016) observed that citric acid adsorption onto goethite generally increased with decreasing pH [28]. For comparison purposes, the ratio q_{max} at pH4 / q_{max} at pH 7 was calculated and presented in Figure 3. Overall, the influence of pH for the studied compounds was more significant with TiO_2 than with Al_2O_3 and ZrO_2 (i.e., expressed by a higher ratio); except for ZrO_2 with citric acid and 4-phenylbutyric acid, showing the highest ratios among the three MeO (i.e., 4.64 and 3.15, respectively). pH exerted a strong influence on citric acid with ZrO_2 and Al_2O_3 (i.e., ratio: 4.64 and 1.9, respectively), and oxalic acid with TiO_2 (ratio: 2.6). Benzoic acid showed a lower ratio with ZrO_2 (0.69), as well as oxalic acid with Al_2O_3 (0.74), and 1, 2-Phenylenediacetic acid with TiO_2 (1.12).

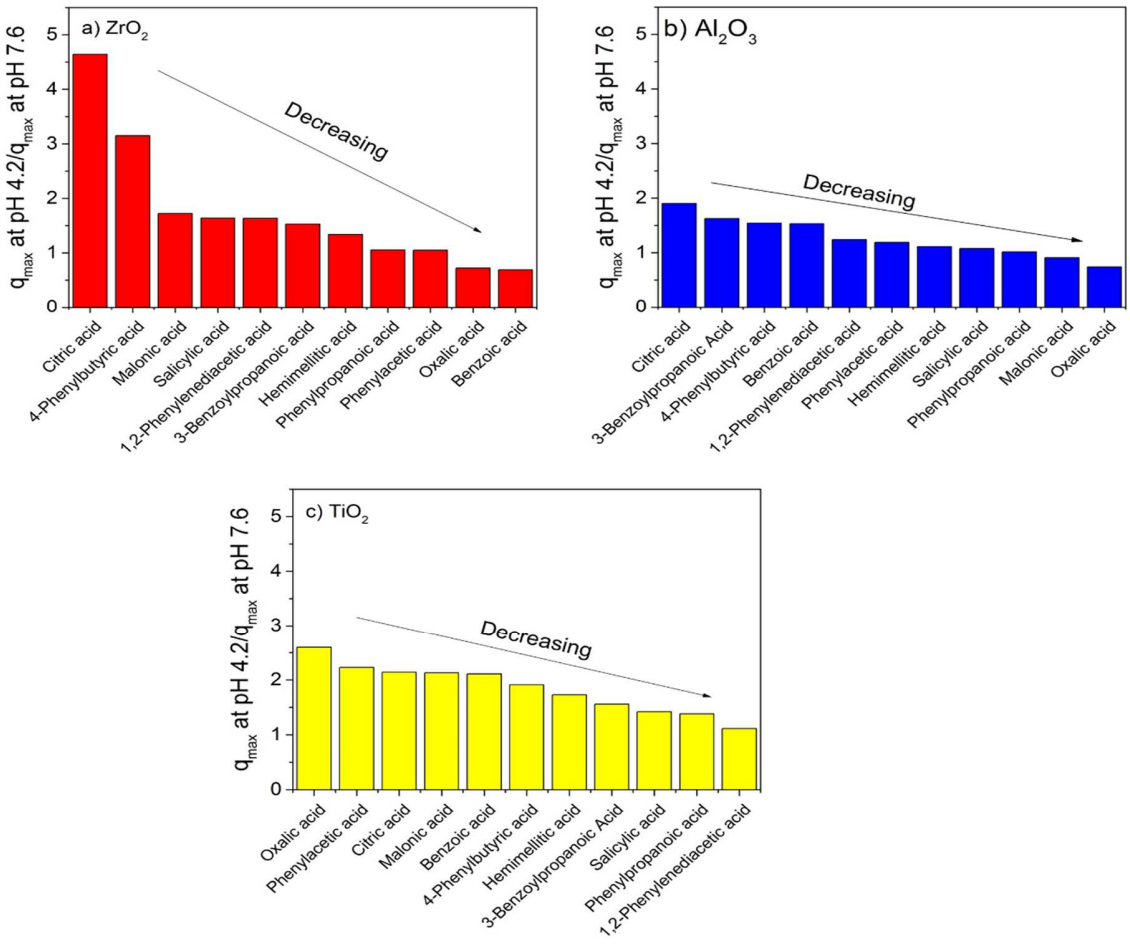

Figure 4: Influence of pH on q_{max} presented as a q_{max} at pH 4.2/q_{max} at pH 7.6 ratio

The highest q_{max} value was obtained with citric acid and ZrO_2 and TiO_2 at pH 4.2 (Figure 4). Except for Al_2O_3 at pH 4.2 and 7.6, 3-Benzoylpropanoic acid showed a higher q_{max} than citric acid (7.44 µmol/m^2 and 4.45 µmol/m^2, respectively). Al_2O_3 showed the highest q_{max} with phenyl carboxylic acids at both pH conditions and with all MeO samples (Table 2). At both pHs, the highest q_{max} was observed with 3-benzoylpropanoic acid. At pH 4.2, Phenylacetic acid showed the lowest q_{max}, while 1,2-phenylenediacetic showed the lowest q_{max} at pH 7.6. At both pH conditions, q_{max} of 1,2-phenylenediacetic acid on MeO surfaces followed the trend: Al_2O_3>TiO_2>ZrO_2, while phenylacetic acid showed the lowest affinity at both pH conditions

following the order of Al_2O_3>TiO_2>ZrO_2 at pH 4.2 and Al_2O_3>ZrO_2>TiO_2 at pH 7.6. The highest maximum adsorption was recorded for 4-phenylbutyric acid with ZrO_2, and then with TiO_2.

pH 4.2	ZrO_2		Al_2O_3		TiO_2
6.08	Citric acid	7.24	3-Benzoylpropanoic Acid	5.45	Citric acid
3.59	4-Phenylbutyric acid	6.64	Citric acid	3.86	4-Phenylbutyric acid
1.99	Hemimellitic acid	4.72	4-Phenylbutyric acid	3.03	3-Benzoylpropanoic Acid
1.63	Phenylpropanoic acid	4.02	1,2-Phenylenediacetic acid	2.51	Hemimellitic acid
1.58	Oxalic acid	3.99	Phenylpropanoic acid	2.25	1,2-Phenylenediacetic acid
1.52	1,2-Phenylenediacetic acid	3.16	Phenylacetic acid	2.15	Malonic acid
1.44	Salicylic acid	1.25	Hemimellitic acid	1.95	Oxalic acid
1.44	3-Benzoylpropanoic acid	1.08	Malonic acid	1.70	Phenylpropanoic acid
1.31	Malonic acid	0.71	Oxalic acid	1.45	Salicylic acid
1.04	Phenylacetic acid	0.67	Salicylic acid	1.15	Phenylacetic acid
0.27	Benzoic acid	0.29	Benzoic acid	0.95	Benzoic acid

pH 7.6	ZrO_2		Al_2O_3		TiO_2
2.18	Oxalic acid	4.45	3-Benzoylpropanoic Acid	2.55	Citric acid
1.55	Phenylpropanoic acid	3.92	Phenylpropanoic acid	2.02	4-Phenylbutyric acid
1.48	Hemimellitic acid	3.49	Citric acid	2.02	1,2-Phenylenediacetic acid
1.31	Citric acid	3.24	1,2-Phenylenediacetic acid	1.95	3-Benzoylpropanoic Acid
1.14	4-Phenylbutyric acid	3.06	4-Phenylbutyric acid	1.45	Hemimellitic acid
0.99	Phenylacetic acid	2.66	Phenylacetic acid	1.23	Phenylpropanoic acid
0.94	3-Benzoylpropanoic acid	1.19	Malonic acid	1.02	Salicylic acid
0.93	1,2-Phenylenediacetic acid	1.13	Hemimellitic acid	1.01	Malonic acid
0.88	Salicylic acid	0.96	Oxalic acid	0.75	Oxalic acid
0.76	Malonic acid	0.62	Salicylic acid	0.52	Phenylacetic acid
0.39	Benzoic acid	0.19	Benzoic acid	0.45	Benzoic acid

Figure 5: Summary of q_{max} of all compounds with Al_2O_3, TiO_2, and ZrO_2 at pH 4.2 and 7.6.

At pH 4.2, the adsorption density was higher with ZrO_2 and TiO_2 than with Al_2O_3, except for citric acid (Table 3). Citric acid showed the strongest adsorption on all MeO samples (i.e., 6.62, 6.08, and 5.45 µmol/m^2 for Al_2O_3, ZrO_2, and TiO_2, respectively). Citric acid (i.e., aliphatic structure) and hemimellitic acid (aromatic structure) generally showed the highest affinities toward all MeO at both pH conditions (Table 3). Conversely, benzoic acid showed the lowest adsorption on all MeO samples at acidic pH (i.e., 0.27, 0.29, and 0.95 µmol/m^2 for ZrO_2, Al_2O_3, and TiO_2, respectively). Malonic, oxalic, and salicylic acids showed relatively similar affinities

346 for MeO (Table 3). q_{max} value for Al_2O_3 and TiO_2 at both pH conditions follows the order of
347 malonic acid > oxalic acid > salicylic acid, except for TiO_2 at pH 7.6, where salicylic acid
348 showed a higher q_{max} than oxalic acid (1.02 µmol/m^2 vs. 0.75 µmol/m^2, respectively). For ZrO_2,
349 q_{max} followed the order of oxalic acid >salicylic acid > malonic acid at both pH conditions.
350 Interestingly, the adsorption density of oxalic acid (2.18 µmol/m^2 and 1.58 µmol/m^2,
351 respectively) and benzoic acid (0.39 µmol/m^2 and 0.27 µmol/m^2, respectively) with ZrO_2 were
352 relatively higher at pH 7.6 than at pH 4.2. Similar results were observed for Al_2O_3, where the
353 adsorption density was slightly higher for oxalic (0.96 µmol/m^2 and 0.71 µmol/m^2, respectively)
354 and malonic acid (1.19 µmol/m^2 and 1.08 µmol/m^2, respectively) at pH 7.6 than at pH 4.2.
355 Briefly, the mechanism of adsorption of the small organic acids on the metal oxide surface is
356 controlled by the pH and pKa. At acidic pH, surface complexation (i.e., ligand exchange) is the
357 main mechanism that controls the adsorption. Ligand exchange refers specifically to direct bond
358 formation (i.e., formation of an inner-sphere complex) between a carboxylate group and metal
359 ion center in metal oxide surface possessing inorganic hydroxyl groups. The effect of pH on the
360 adsorption isotherms showed a behavior typically observed for anion adsorption, specifically,
361 high adsorption at low pH, which decreases with increasing pH. Because all MeO samples are
362 positively charged at acidic conditions and most of the investigated acids contained at least one
363 carboxylic group (i.e., pK_a value ranging from 1-5) [20, 22, 39], the adsorption of these acids
364 was mainly controlled by electrostatic interactions and by surface complexation mechanisms [33,
365 39]. The free energy of ions adsorption contributing to the electrostatic interactions is relatively
366 small; thus, electrostatic interactions would have a lower contribution to the adsorption
367 mechanism [20, 40]. Regarding surface complexation, Evanko and Dzombak (1998) stated that
368 at high pH, the surface of iron oxide is negatively charged, and surface oxygen atoms are tightly

bound and are less likely to interact with acidic functional groups in solution. As pH decreases, neutral and positively charged surface sites are formed, the iron-oxygen bond is weakened due to decreased electron density of the bond, and the oxygens are exchanged with functional groups of the organic acids as OH- or OH_2 [20].

The chemical structure, number of COOH groups, and carbon chain of the saturated fatty acid of the studied organic acids showed a significant influence on the adsorption density onto MeO. An additional carboxyl or hydroxyl group on the aromatic ring enhanced the adsorption affinity on Al_2O_3, TiO_2, and ZrO_2 (e.g., compared to benzoic acid with only one carboxyl group). Similarly, an increased number of COOH groups increased the adsorption on the MeO surface, e.g., citric acid (triprotic) and malonic acid (diprotic) (Figure 6a), suggesting that additional surface complexes may form on MeO [20, 34]. Compounds with the lowest pK_a are overall considered more acidic. For compounds with multiple acidic functional groups (i.e., multiple pK_a), the acidity of additional functional groups must be assessed at both pH conditions because more than one functional group could be involved in the adsorption [20, 34]. Non dissociated carboxyl groups (pK_a>pH) could contribute and enhance the molecule adsorption on the MeO surface [41].

The increase in the adsorption may also result from increasing the acidity of the acid molecule (i.e., carboxyl group) [33]. Thus, the structure of salicylic acid would provide more adsorption energy on the MeO surface compared to benzoic acid by increasing the acidity of COOH with the presence of an OH group in the ortho position. Guan et al. (2006) observed that the presence of OH groups on the aromatic ring increases the interaction between carboxylate and Al_2O_3. Because the phenolic groups have a strong electron-donating resonance effect [42], their

presence near the carboxyl group can increase the electron density within the carboxyl group; therefore, favoring the metal-carboxylate complexation [43].

The acidity of organic acids strongly influences their adsorption behavior. Das and Mahiuddin (2005) reported that the higher adsorption density of phthalate on the α-Al_2O_3 surface compared to benzoic acid was due to the adjacent carboxylic group [34]. Vasudevan and Stone (1996) suggested that the nature of the substituents to organic acids can have a significant effect on the adsorption properties of organic ligands by influencing the acidity. In their study of the adsorption of aromatic amines onto MeO, the presence of electron-withdrawing substituents lowered the basicity of the aromatic amines at donor groups and shifted the maximum adsorption to more acidic pH values [28]. Edwards and Benjamin (1996) observed that organic matter with considerably strong acid groups (i.e., groups ionized below pH 3) was preferentially adsorbed to goethite compared to organic matter with weaker acid groups, suggesting that strong acid groups are essential for controlling NOM sorption to MeO [44]. These findings are in agreement with previous studies of adsorption of simple organic acids in which poly-protic acids having at least one considerably strong acid group (e.g., malonic, oxalic, and hemimellitic acids) strongly adsorbed to MeO surfaces; whereas the adsorption of mono-protic acids without strong acid groups (benzoic acid) showed a significantly weaker affinity [20, 37, 38, 44].

The aliphatic structures would exert higher adsorption on MeO than aromatic structures (Figure 6a-b) under similar acidic character (e.g., citric acid versus hemimellitic acid), indicating that the conformation of the molecule (access to adsorption sites) plays an important role. This conformation effect is also observed when comparing the adsorption of oxalic acid (C2 diprotic) and malonic acid (C3 diprotic) (Figure 6a), except for ZrO_2. By increasing the length of the molecule, the adsorption affinity of the aliphatic compounds on Al_2O_3, TiO_2, and ZrO_2 also

increased. Dobson and McQuilln (2000) reported that the adsorption of aliphatic dicarboxylic acid was sensitive to the carbon-chain length of the adsorbate. They showed that long-chain adsorbates (C4 and larger) exhibited high molecular flexibility, allowing the formation of tetradentate looped surface structures. Short-chain adsorbates (C2 and C3) exhibited low molecular flexibility; thus, they are unable to form a tetradentate surface structure that strongly adsorbs to MeO forming side-on coordinated species through ester linkages involving each of the carboxylate functional groups [18].

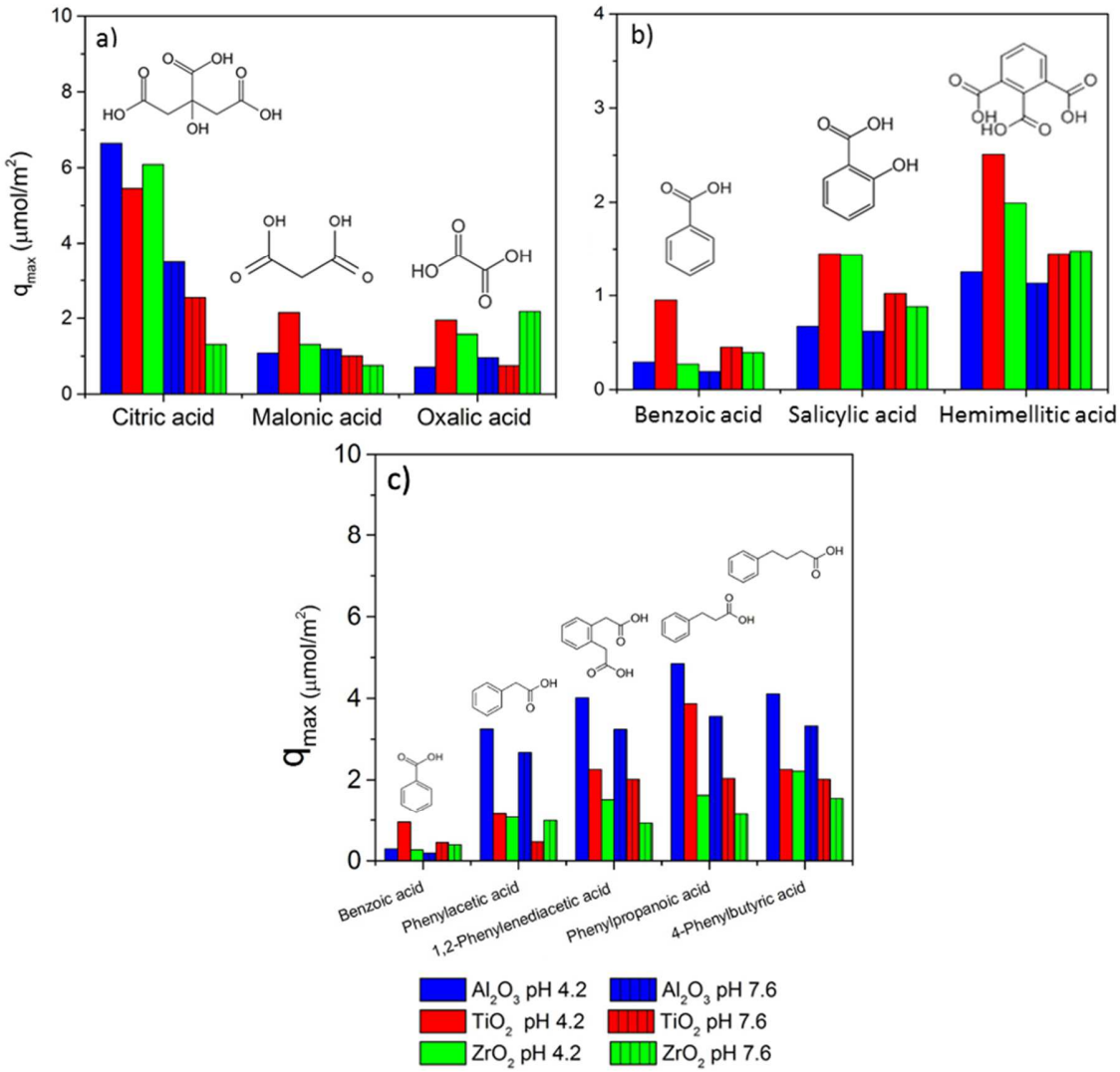

Figure 6. Influence of chemical structure on the adsorption density qmax value of a) aliphatic acids and, b) aromatic acids, c) presence of alkyl chain and its length on phenyl carboxylic acids onto MeO surface

The length of the carbon chain of the saturated fatty acid attached to a phenyl group also influences the adsorption onto MeO (Figure 6c). Results showed that for all MeO, the longer the fatty acid (e.g., phenylacetic, phenylpropionic, and phenylbutyric acids), the higher the q_{max} value. This increase in adsorption may involve the interaction of the carboxyl group and also the hydrophobic moieties of the molecule [20]. The pK_a values of COOH are relatively similar (i.e., 4.2, 4.31, 4.37, and 4.76 for benzoic acid, phenylacetic acid, phenylpropanoic acid, and 4-phenylbutyric acid, respectively) (Figure 6c). The adsorption density increased with the length of the carbon chain carrying the carboxyl group. Besides, the length of the carbon chain is more influential in the adsorption density than an additional carboxyl group in the phenyl structure (i.e., 1, 2 phenylenediacetic acid vs. phenylpropanoic acid). Previous studies have suggested that the hydrophobic contribution to the adsorption may cause some organic acids to adsorb by more than one layer on the oxide surface; thus, the surface coverage may be increased [45, 46]. The effect of hydrophobic interactions on the adsorption to MeO has been investigated with surfactant molecules. Wakamatsu and Fuerstenau (1968) found that increasing the hydrocarbon chain length of alkyl sulfonates enhanced the adsorption in alumina, resulting in high sorption densities for the larger molecules relative to the smaller molecules [47].

3.4. Influence of the surface characteristics of the MeO on the adsorption on organic acids

The MeO properties have a significant influence on the adsorption of organic acids. Several properties of MeO exert an impact on the adsorption density of small organic acids: surface area, charge density, and type of hydroxyl group exposed on the surface [35, 36, 48]. The density of the positive charges or charge density on the solid is more important than the charge of the

447 organic acid. pH has a key influence on the surface charge of MeO. From the pH_{PZC} curves,
448 Al_2O_3 and TiO_2 evidence a higher charge density than ZrO_2 (Figure S1), a characteristic that
449 explains the higher adsorption efficiency of Al_2O_3 and TiO_2 with some organic acids as
450 compared to ZrO_2. As an example, salicylic acid showed a higher adsorption affinity on the
451 Al_2O_3 surface (14.37) than on TiO_2 (1.31) and ZrO_2 (0.25) at acidic pH. Interestingly, by
452 increasing the pH, the affinity of benzoic acid toward the MeO surface increased with all MeO
453 (i.e., especially with ZrO_2), which could be related to a modification of the adsorption
454 mechanism [22].
455 The positive charge controls the interaction mechanism and the affinity of the organic acids with
456 the MeO surface by either ligand exchange or electrostatic interactions [49]. This can be
457 evidenced by the slight increase of pH in the adsorption process and would indicate the replacing
458 of the OH^+ group on the metal surface by the COOH group on the acid [35].
459 The type and nature of active sites present on the MeO surface are also important factors that
460 contribute to the adsorption of small organic acids. As most of the studied acids are carboxylic
461 acids, the reactions that control the adsorption are mainly in the form of acid-base mechanisms.
462 A Brønsted acid-base formation provides a good description of the dissociative adsorption of this
463 group of acids (Figure 1). Most MeO expose cation-anion pairs. These are the active sites for this
464 type of reaction, which proceeds through the adsorption of the acidic proton by a surface O^{2-}
465 anion to form an adsorbed hydroxyl group with the conjugate base anion of the organic acids
466 bonding to an exposed metal cation. The relative acid-base strength of oxide surfaces is
467 proportional to their ability to dissociate Brønsted acids [36, 50, 51]. According to TPD (Table
468 S1), Al_2O_3 and TiO_2 surfaces are mainly predominant with strong sites per surface area
469 compared to ZrO_2. Therefore, the adsorption of some organic acid, e.g., Phenylacetic acid and

benzoic acid, tends to decrease in contact with ZrO_2 as it shows weaker sites than TiO_2. Besides, the local coordination environment of the cations-anions pairs plays an essential role. In many cases, this requirement can lead to high structural sensitivities, including large variations in reactivity for different exposed crystal planes in a single MeO [36, 50]. Several studies have reported that the most important active sites on the surface of MeO in the adsorption process are OH^- groups [48, 52, 53]. Two types of OH^- groups are formed on the surface of MeO, one with surface oxygen and the other one on metal cation surface [30]. Each MeO exerts a different density of OH^- with various configurations on the surface of MeO as described by Tsyganenko and Filimonov [32] and Hering [54].

Surface hydroxyl oxygen can be bound to 1, 2, or 3 metal atoms. Therefore, the nature of the cation-anion pairs on the surface of Al_2O_3, TiO_2, and ZrO_2 is determined by their crystallinity [36]. According to the characterization of the MeO samples by XRD, ZrO_2 has a monoclinic crystal structure with particles of (110) or (101) planes. The reported types of hydroxyl sites on this structure are mono-coordinate and tri-bridge OH groups [30]. The presence of two different types of ZrO_2 particles might lead to different adsorption densities because each plane provides the particles with different surface characters [32]. TiO_2 is in the rutile phase in the (101) plane, where type I and II hydroxyl groups would be expected [32]. The crystallinity of Al_2O_3 particles is in the corundum form in the phase (11-20), and the possible hydroxyl groups are I, II, and II [53]. Based on several parameters (i.e., type of MeO, crystallinity, and processing the MeO), different densities of each type are exposed on the surface [55-57]. Based on the type of OH^- on the surface, different affinities of organic acids would be observed [57].

4. Conclusions

The adsorption of carboxylic acids and phenylcarboxylic acids on MeO particles followed the Langmuir isotherm model; thus, indicating monolayer adsorption. Generally, the degree of adsorption density of these small organic acids on MeO was influenced by the MeO surface charge, pK_a, chemistry of the adsorbate, and pH. Typically, at acidic pH of 4.2, the maximum adsorption of the organic acids on Al_2O_3, TiO_2, and ZrO_2 was higher compared to pH 7.6. Except for malonic and oxalic acids, as they showed the opposite trend, which could be related to their molecular structure. The pH affected the ionization state of the organic acids and the surface charge on MeO.

Increasing the acidity of the organic molecule, either by increasing the number of COOH groups (i.e., citric acid) or by the presence of OH groups (salicylic acid vs. benzoic acid), increased the adsorption density on MeO at acidic and neutral pH. Different conformation of the organic acid, i.e., aliphatic or aromatic structure (citric acid vs. hemimellitic acid), and the length of the aliphatic acids (oxalic vs. malonic acids) influenced the adsorption on MeO. Phenyl carboxylic acids showed a high adsorption affinity on all MeO surfaces. Also, the presence of a carbon chain of saturated fatty acid was more important than COOH groups in phenyl acids (phenylacetic, phenylpropionic, and phenylbutyric acids). Finally, different surface characteristics of MeO prompted various maximum adsorption of the organic acids, i.e., the density of the active site (basic and acidic sites) and $pH_{PZC.}$ The results of the current study would have key implications on ceramic membrane fouling. Although highly dependent on surface characteristics, for the MeO tested, higher adsorption of organics (i.e., leading to fouling) would be expected at acidic pH. However, at neutral pH (i.e., mimicking major environmentally relevant conditions), the adsorption of organics would be lower; thus, providing deep insight on optimum operational conditions.

Acknowledgment

The authors are grateful to KAUST for the support of the project, Manuel A. Roldan for analyzing the TEM images, and Tao Zhang for the scientific support in developing the HLPC methods.

References

1. Mourouzidis-Mourouzis, S. and A. Karabelas, *Whey protein fouling of large pore-size ceramic microfiltration membranes at small cross-flow velocity.* Journal of Membrane Science, 2008. **323**(1): p. 17-27.
2. Masheane, M., et al., *Physico-chemical characteristics of some Lesotho's clays and their assessment for suitability in ceramics production.* Particulate Science and Technology, 2018. **36**(1): p. 117-122.
3. Baker, R.W., *Membrane technology and applications*. 2012: John Wiley & Sons.
4. Urbanowska, A. and M. Kabsch-Korbutowicz, *Influence of operating conditions on performance of ceramic membrane used for water treatment.* Chemical Papers, 2014. **68**(2): p. 190-196.
5. Arhin, S.G., et al., *Membrane fouling control in low pressure membranes: A review on pretreatment techniques for fouling abatement.* Environmental Engineering Research, 2016. **21**(2): p. 109-120.
6. Li, W., et al., *Ceramic membrane fouling and cleaning during ultrafiltration of limed sugarcane juice.* Separation and Purification Technology, 2018. **190**: p. 9-24.
7. Zhu, H., X. Wen, and X. Huang, *Characterization of membrane fouling in a microfiltration ceramic membrane system treating secondary effluent.* Desalination, 2012. **284**: p. 324-331.
8. Leenheer, J.A. and J.-P. Croué, *Peer reviewed: Characterizing aquatic dissolved organic matter.* Environmental Science & Technology, 2003. **37**(1): p. 18A-26A.
9. Croué, J.-P., *Isolation of humic and non-humic NOM fractions: structural characterization.* Environmental monitoring and assessment, 2004. **92**(1-3): p. 193-207.
10. Leenheer, J.A., et al., *Characterization and origin of polar dissolved organic matter from the Great Salt Lake.* Biogeochemistry, 2004. **69**(1): p. 125-141.
11. Leenheer, J.A., *Systematic approaches to comprehensive analyses of natural organic matter.* Ann. Environ. Sci, 2009. **3**(1): p. e130.
12. Liu, T., et al., *Mitigation of NOM fouling of ultrafiltration membranes by pre-deposited heated aluminum oxide particles with different crystallinity.* Journal of Membrane Science, 2017. **544**: p. 359-367.
13. Gu, B., et al., *Adsorption and desorption of natural organic matter on iron oxide: mechanisms and models.* Environmental Science & Technology, 1994. **28**(1): p. 38-46.
14. Claret, F., et al., *Fractionation of Suwannee River fulvic acid and Aldrich humic acid on α-Al2O3: Spectroscopic evidence.* Environmental Science & Technology, 2008. **42**(23): p. 8809-8815.

15. Kummert, R. and W. Stumm, *The surface complexation of organic acids on hydrous γ-Al2O3.* Journal of Colloid and Interface Science, 1980. **75**(2): p. 373-385.
16. Korshin, G.V., M.M. Benjamin, and R.S. Sletten, *Adsorption of natural organic matter (NOM) on iron oxide: effects on NOM composition and formation of organo-halide compounds during chlorination.* Water Research, 1997. **31**(7): p. 1643-1650.
17. Weng, L., W.H. Van Riemsdijk, and T. Hiemstra, *Adsorption of humic acids onto goethite: Effects of molar mass, pH and ionic strength.* Journal of Colloid and Interface Science, 2007. **314**(1): p. 107-118.
18. Dobson, K.D. and A.J. McQuillan, *In situ infrared spectroscopic analysis of the adsorption of aromatic carboxylic acids to TiO2, ZrO2, Al2O3, and Ta2O5 from aqueous solutions.* Spectrochimica Acta Part A: Molecular and Biomolecular Spectroscopy, 2000. **56**(3): p. 557-565.
19. Meier, M., et al., *Fractionation of aquatic natural organic matter upon sorption to goethite and kaolinite.* Chemical geology, 1999. **157**(3-4): p. 275-284.
20. Evanko, C.R. and D.A. Dzombak, *Influence of structural features on sorption of NOM-analogue organic acids to goethite.* Environmental science & technology, 1998. **32**(19): p. 2846-2855.
21. Dobson, K.D. and A.J. McQuillan, *In situ infrared spectroscopic analysis of the adsorption of aliphatic carboxylic acids to TiO2, ZrO2, Al2O3, and Ta2O5 from aqueous solutions.* Spectrochimica Acta Part A: Molecular and Biomolecular Spectroscopy, 1999. **55**(7-8): p. 1395-1405.
22. Hwang, Y.S. and J.J. Lenhart, *Adsorption of C4-dicarboxylic acids at the hematite/water interface.* Langmuir, 2008. **24**(24): p. 13934-13943.
23. Borah, J.M. and S. Mahiuddin, *Adsorption and surface complexation of trimesic acid at the α-alumina–electrolyte interface.* Journal of colloid and interface science, 2008. **322**(1): p. 6-12.
24. Kosmulski, M., *Compilation of PZC and IEP of sparingly soluble metal oxides and hydroxides from literature.* Advances in colloid and interface science, 2009. **152**(1-2): p. 14-25.
25. Sivaraj, C., C. Contescu, and J. Schwarz, *Effect of calcination temperature of alumina on the adsorption/impregnation of Pd (II) compounds.* Journal of Catalysis, 1991. **132**(2): p. 422-431.
26. Zhang, H. and J.F. Banfield, *Phase transformation of nanocrystalline anatase-to-rutile via combined interface and surface nucleation.* Journal of Materials Research, 2000. **15**(2): p. 437-448.
27. Ahonen, P., et al., *Preparation of nanocrystalline titania powder via aerosol pyrolysis of titanium tetrabutoxide.* Journal of materials research, 1999. **14**(10): p. 3938-3948.
28. Zaban, A., et al., *The Effect of the Preparation Condition of TiO2 Colloids on Their Surface Structures.* The Journal of Physical Chemistry B, 2000. **104**(17): p. 4130-4133.
29. Yang, H.G., et al., *Anatase TiO 2 single crystals with a large percentage of reactive facets.* Nature, 2008. **453**(7195): p. 638.
30. Kouva, S., et al., *monoclinic zirconia, its surface sites and their interaction with carbon monoxide.* Catalysis science & technology, 2015. **5**(7): p. 3473-3490.

31. Jung, K.T., Y.G. Shul, and A.T. Bell, *The preparation and surface characterization of zirconia polymorphs.* Korean Journal of Chemical Engineering, 2001. **18**(6): p. 992-999.
32. Tsyganenko, A. and V. Filimonov, *Infrared spectra of surface hydroxyl groups and crystalline structure of oxides.* Journal of Molecular structure, 1973. **19**: p. 579-589.
33. Alliot, C., et al., *Sorption of aqueous carbonic, acetic, and oxalic acids onto α-alumina.* Journal of colloid and interface science, 2005. **287**(2): p. 444-451.
34. Das, M.R. and S. Mahiuddin, *Kinetics and adsorption behaviour of benzoate and phthalate at the α-alumina–water interface: Influence of functionality.* Colloids and Surfaces A: Physicochemical and Engineering Aspects, 2005. **264**(1-3): p. 90-100.
35. Honghai, W., et al., *Surface adsorption of iron oxide minerals for phenol and dissolved organic matter.* Earth Science Frontiers, 2008. **15**(6): p. 133-141.
36. Vohs, J.M., *Site requirements for the adsorption and reaction of oxygenates on metal oxide surfaces.* Chemical reviews, 2012. **113**(6): p. 4136-4163.
37. Borah, J.M., J. Sarma, and S. Mahiuddin, *Influence of functional groups on the adsorption behaviour of substituted benzoic acids at the α-alumina/water interface.* Colloids and Surfaces A: Physicochemical and Engineering Aspects, 2011. **375**(1-3): p. 42-49.
38. Balistrieri, L.S. and J.W. Murray, *The influence of the major ions of seawater on the adsorption of simple organic acids by goethite.* Geochimica et Cosmochimica Acta, 1987. **51**(5): p. 1151-1160.
39. Evanko, C.R. and D.A. Dzombak, *Surface complexation modeling of organic acid sorption to goethite.* Journal of colloid and interface science, 1999. **214**(2): p. 189-206.
40. Laxen, D.P., *Trace metal adsorption/coprecipitation on hydrous ferric oxide under realistic conditions: the role of humic substances.* Water Research, 1985. **19**(10): p. 1229-1236.
41. Gocmez, H., *The interaction of organic dispersant with alumina: A molecular modelling approach.* Ceramics international, 2006. **32**(5): p. 521-525.
42. Vasudevan, D. and A.T. Stone, *Adsorption of catechols, 2-aminophenols, and 1, 2-phenylenediamines at the metal (hydr) oxide/water interface: effect of ring substituents on the adsorption onto TiO2.* Environmental science & technology, 1996. **30**(5): p. 1604-1613.
43. Guan, X.-H., C. Shang, and G.-H. Chen, *ATR-FTIR investigation of the role of phenolic groups in the interaction of some NOM model compounds with aluminum hydroxide.* Chemosphere, 2006. **65**(11): p. 2074-2081.
44. Borah, J.M., M.R. Das, and S. Mahiuddin, *Influence of anions on the adsorption kinetics of salicylate onto α-alumina in aqueous medium.* Journal of colloid and interface science, 2007. **316**(2): p. 260-267.
45. Das, M.R. and S. Mahiuddin, *The influence of functionality on the adsorption of p-hydroxy benzoate and phthalate at the hematite–electrolyte interface.* Journal of colloid and interface science, 2007. **306**(2): p. 205-215.
46. Yost, E.C., M.I. Tejedor-Tejedor, and M.A. Anderson, *In situ CIR-FTIR characterization of salicylate complexes at the goethite/aqueous solution interface.* Environmental Science & Technology, 1990. **24**(6): p. 822-828.

47. Gould, R.F., *Adsorption From Aqueous Solution, Copyright, Advances in Chemistry Series, FOREWORD*, in *Adsorption From Aqueous Solution*, F.G. Robert, Editor. 1968, AMERICAN CHEMICAL SOCIETY. p. i-vi.
48. Takeda, S., et al., *Surface OH group governing adsorption properties of metal oxide films.* Thin Solid Films, 1999. **339**(1-2): p. 220-224.
49. Schlautman, M.A. and J.J. Morgan, *Adsorption of aquatic humic substances on colloidal-size aluminum oxide particles: Influence of solution chemistry.* Geochimica et Cosmochimica Acta, 1994. **58**(20): p. 4293-4303.
50. Alsawalha, M., *Characterization of acidic and basic properties of heterogeneous catalysts by test reactions*. 2005, Universität Oldenburg.
51. Barteau, M.A., *Organic reactions at well-defined oxide surfaces.* Chemical reviews, 1996. **96**(4): p. 1413-1430.
52. Zhang, T., et al., *Surface hydroxyl groups of synthetic α-FeOOH in promoting OH generation from aqueous ozone: property and activity relationship.* Applied Catalysis B: Environmental, 2008. **82**(1-2): p. 131-137.
53. Shirai, T., et al., *Structural properties and surface characteristics on aluminum oxide powders.* 2010.
54. Hering, J.G., *Interaction of organic matter with mineral surfaces: Effects on geochemical processes at the mineral-water interface.* Advances in Chemistry Series, 1995. **244**: p. 95-95.
55. Hadjiivanov, K., D. Klissurski, and A. Davydov, *Effect of the surface structure of metal oxides on their adsorption properties.* Journal of the Chemical Society, Faraday Transactions 1: Physical Chemistry in Condensed Phases, 1988. **84**(1): p. 37-40.
56. Boehm, H., *Acidic and basic properties of hydroxylated metal oxide surfaces.* Discussions of the Faraday Society, 1971. **52**: p. 264-275.
57. Chvedov, D. and E.L. Logan, *Surface charge properties of oxides and hydroxides formed on metal substrates determined by contact angle titration.* Colloids and Surfaces A: Physicochemical and Engineering Aspects, 2004. **240**(1-3): p. 211-223.

Table 1. Surface concentration of basic and acidic sites on MeO particles

Temp. (°C)	Acidic sites (µmol/m^2)	Temp. (°C)	Basic sites (µmol/m^2)
Al_2O_3			
363.0	8.85	23.60	2.03
576.0	7.22	19.25	8.14
842.6	3.67	**-**	-
TiO_2			
237.7	17.46	**-**	-
375.3	14.61	**-**	-
581.8	6.31	**-**	-
810.2	4.23	**-**	-
ZrO_2			
291.5	2.45	17.43	0.24
466.2	5.31	37.77	0.33
757.4	2.45	**-**	-

Table 2: Langmuir adsorption isotherm parameters of phenyl carboxylic acids calculated from Equation 3.

*q_{max}: µmol/m²	pH 4.2			pH 7.6				
	q_{max}*	K	R^2	q_{max}*	K	R^2	$q_{max\ 4.2}/q_{max\ 7.6}$	$K_{4.2}/K_{7.6}$
	ZrO_2							
Phenylacetic acid	1.04	2.81	0.91	0.99	2.28	0.91	1.05	1.23
1,2-Phenylenediacetic acid	1.52	3.14	0.98	0.93	0.59	0.94	1.63	5.32
Phenylpropanoic acid	1.63	0.21	0.91	1.55	2.61	0.96	1.06	0.08
4-Phenylbutyric acid	3.59	0.09	0.91	1.14	2.63	0.89	3.15	0.03
3-Benzoylpropanoic acid	1.44	0.37	0.98	0.94	0.65	0.88	1.53	0.57
	Al_2O_3							
Phenylacetic acid	3.16	2.94	0.99	2.66	1.32	0.92	1.19	2.22
1,2-Phenylenediacetic acid	4.02	1.36	0.94	3.24	0.26	0.93	1.24	5.16
Phenylpropanoic acid	3.99	0.67	0.85	3.92	0.84	0.8	1.02	0.81
4-Phenylbutyric acid	4.72	2.42	0.93	3.06	0.41	0.94	1.54	5.84
3-Benzoylpropanoic Acid	7.24	0.12	0.94	4.45	0.81	0.93	1.63	0.15
	TiO_2							
Phenylacetic acid	1.16	1.45	0.82	0.52	0.71	0.94	2.23	2.03
1,2-Phenylenediacetic acid	2.26	0.68	0.95	2.02	1.06	0.92	1.12	0.65
Phenylpropanoic acid	1.71	0.87	0.96	1.23	0.49	0.9	1.38	1.80
4-Phenylbutyric acid	3.87	0.30	0.92	2.02	14.18	0.83	1.91	0.02
3-Benzoylpropanoic Acid	3.04	0.63	0.9	1.95	0.15	0.94	1.56	4.29

Table 3: Langmuir adsorption isotherm parameters of carboxylic acids and phenylcarboxylic acids calculated from Equation 3.

	ZrO_2							
$*q_{max}$: µmol/m²	pH 4.2			pH 7.6				
	q_{max}*	k	R^2	q_{max}*	k	R^2	$q_{max4.2}/q_{max\ 7.6}$	$K_{4.2}/K_{7.6}$
Citric acid	6.08	0.29	0.87	1.31	0.66	0.91	4.64	0.44
Malonic acid	1.31	0.88	0.97	0.76	0.37	0.89	1.72	2.4
Oxalic acid	1.58	0.8	0.85	2.18	0.13	0.99	0.72	6
Benzoic acid	0.27	3.31	0.94	0.39	15.45	0.91	0.69	0.21
Salicylic acid	1.44	0.25	0.88	0.88	1.11	0.92	1.64	0.23
Hemimellitic acid	1.99	0.33	0.98	1.48	0.25	0.91	1.34	1.34
	Al_2O_3							
Citric acid	6.64	0.25	0.87	3.49	1.59	0.87	1.9	0.16
Malonic acid	1.08	11.56	0.85	1.19	9.9	0.9	0.91	1.17
Oxalic acid	0.71	2.16	0.85	0.96	44.44	0.87	0.74	0.049
Benzoic acid	0.29	3.08	0.85	0.19	13.47	0.83	1.53	0.23
Salicylic acid	0.67	14.37	0.87	0.62	17.14	0.86	1.08	0.84
Hemimellitic acid	1.25	11.09	0.94	1.13	5.04	0.89	1.11	2.2
	TiO_2							
Citric acid	5.45	0.2	0.91	2.55	0.85	0.93	2.14	0.24
Malonic acid	2.15	1.19	0.87	1.01	0.47	0.93	2.13	2.55
Oxalic acid	1.95	0.28	0.97	0.75	0.04	0.97	2.6	6.45
Benzoic acid	0.95	0.36	0.83	0.45	1.35	0.85	2.11	0.26
Salicylic acid	1.45	1.31	0.96	1.02	1.02	0.88	1.42	1.28
Hemimellitic acid	2.51	0.19	0.98	1.45	1.93	0.89	1.73	0.1

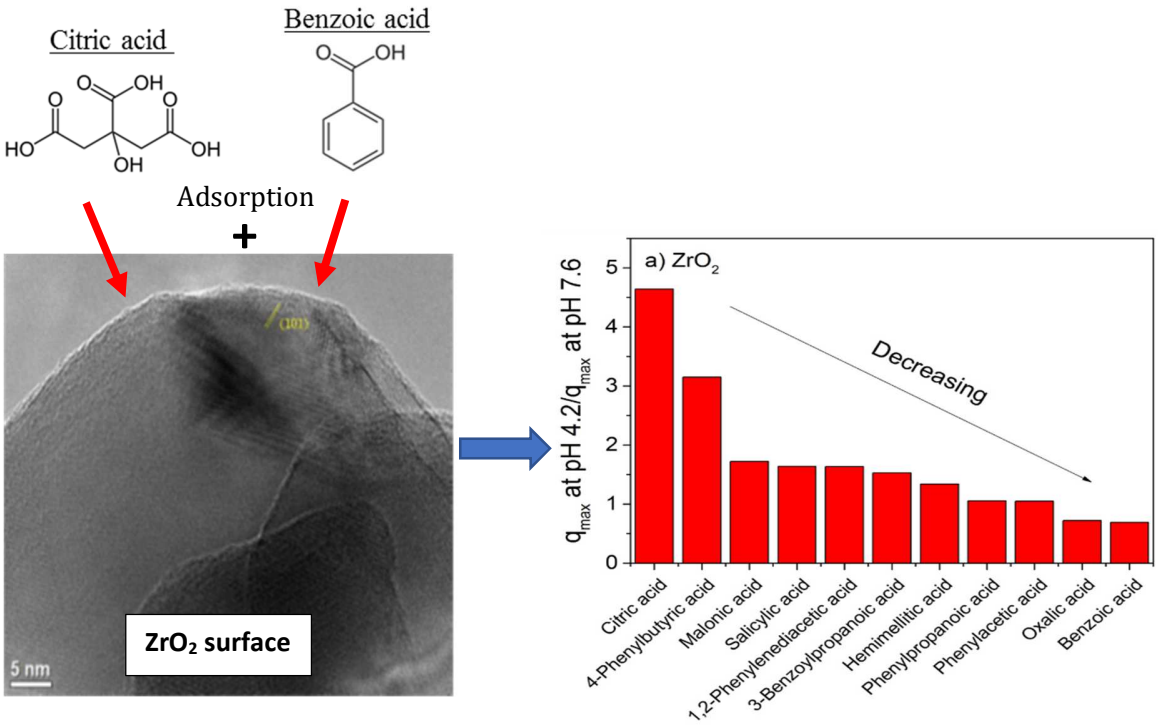
Citric acid
Benzoic acid
Adsorption
+
ZrO2 surface
5 nm
a) ZrO2
Decreasing
qmax at pH 4.2/qmax at pH 7.6
Citric acid
4-Phenylbutyric acid
Malonic acid
Salicylic acid
1,2-Phenylenediacetic acid
3-Benzoylpropanoic acid
Hemimellitic acid
Phenylpropanoic acid
Phenylacetic acid
Oxalic acid
Benzoic acid